01 Nov 2014

Modeling of Thermal and Mechanical Behavior of ZrB_2-SiC Ceramic After High Temperature Oxidation

Jun Wei
Missouri University of Science and Technology, junwei@mst.edu

Lokeswarappa R. Dharani
Missouri University of Science and Technology, dharani@mst.edu

K. Chandrashekhara
Missouri University of Science and Technology, chandra@mst.edu

Greg Hilmas
Missouri University of Science and Technology, ghilmas@mst.edu

et. al. For a complete list of authors, see https://scholarsmine.mst.edu/mec_aereng_facwork/3725

Recommended Citation

J. Wei et al., "Modeling of Thermal and Mechanical Behavior of ZrB_2-SiC Ceramic After High Temperature Oxidation," *Journal of Ceramics*, vol. 2014, Hindawi Publishing Corporation, Nov 2014.
The definitive version is available at https://doi.org/10.1155/2014/169748

Hindawi Publishing Corporation
Journal of Ceramics
Volume 2014, Article ID 169748, 9 pages
http://dx.doi.org/10.1155/2014/169748

Research Article

Modeling of Thermal and Mechanical Behavior of ZrB_2-SiC Ceramics after High Temperature Oxidation

Jun Wei,[1] Lokeswarappa R. Dharani,[1] K. Chandrashekhara,[1] Gregory E. Hilmas,[2] and William G. Fahrenholtz[2]

[1] *Department of Mechanical and Aerospace Engineering, Missouri University of Science and Technology, Rolla, MO 65409-0050, USA*
[2] *Department of Materials Science and Engineering, Missouri University of Science and Technology, Rolla, MO 65409-0340, USA*

Correspondence should be addressed to Lokeswarappa R. Dharani; dharani@mst.edu

Received 31 July 2014; Accepted 18 October 2014; Published 11 November 2014

Academic Editor: Guillaume Bernard-Granger

The effects of oxidation on heat transfer and mechanical behavior of ZrB_2-SiC ceramics at high temperature are modeled using a micromechanics based finite element model. The model recognizes that when exposed to high temperature in air ZrB_2-SiC oxidizes into ZrO_2, SiO_2, and SiC-depleted ZrB_2 layer. A steady-state heat transfer analysis was conducted at first and that is followed by a thermal stress analysis. A "global-local modeling" technique is used combining finite element with infinite element for thermal stress analysis. A theoretical formulation is developed for calculating the thermal conductivity of liquid phase SiO_2. All other temperature dependent thermal and mechanical properties were obtained from published literature. Thermal stress concentrations occur near the pore due to the geometric discontinuity and material properties mismatch between the ceramic matrix and the new products. The predicted results indicate the development of thermal stresses in the SiO_2 and ZrO_2 layers and high residual stresses in the SiC-depleted ZrB_2 layer.

1. Introduction

Ultrahigh temperature ceramics (UHTCs) such as zirconium diboride and hafnium diboride (ZrB_2 and HfB_2) have been proposed for thermal protection of hypersonic aerospace vehicles, which may be exposed to temperatures above 1500°C in oxidizing environments. These materials are chemically and physically stable above 1600°C and have melting points above 3000°C [1]. In particular, ZrB_2 because of its lower theoretical density is attractive for aerospace applications [2]. Exposure of solid zirconium boride (ZrB_2 (s)) to air at elevated temperatures results in its oxidation to solid zirconia (ZrO_2 (s)) and liquid boria (B_2O_3 (l)). The oxidation resistance of ZrB_2 (s) can be improved by adding SiC (s) to promote the formation of a silica-rich scale. At high temperature, above 1100°C, SiC (s) oxidizes by reaction to form SiO_2 (l) which has a lower volatility and a higher melting point and viscosity compared with B_2O_3 (l) [3–5]. Based on the experimental observations, Fahrenholtz [3] proposed a reaction sequence for the formation of the SiC-depleted layer during the oxidation of ZrB_2-SiC at 1500°C in air. The oxide scales that form on ZrB_2-SiC consist of an outer layer of SiO_2, a middle layer of porous ZrO_2, sometimes filled with SiO_2, and a layer of SiC-depleted ZrB_2 adjoining the unoxidized ZrB_2-SiC at around 1500°C [2–6]. Parthasarathy et al. [7] developed a chemical reaction model for the oxidation of ZrB_2-SiC ceramics to predict the thicknesses of the above three new productions. For temperatures below ~1600°C, an external glassy SiO_2 layer forms and completely fills in pores of the porous ZrO_2 scale whereas at higher temperatures, the glassy scale recedes due to evaporation of SiO_2 (l) so that it only partially fills the pores in the ZrO_2 layer.

The region of particular interest, from a mechanical perspective, is the interface between the pores and the corner of the pores in the ZrO_2 scale. The pore itself may or may not be filled with liquid SiO_2 (l). The interface therefore consists of three materials (ZrO_2 scale, solid/liquid SiO_2, and SiC-depleted ZrB_2 layer) of significantly different thermal and mechanical properties. This thermomechanical mismatch and geometric discontinuity would lead to residual stresses,

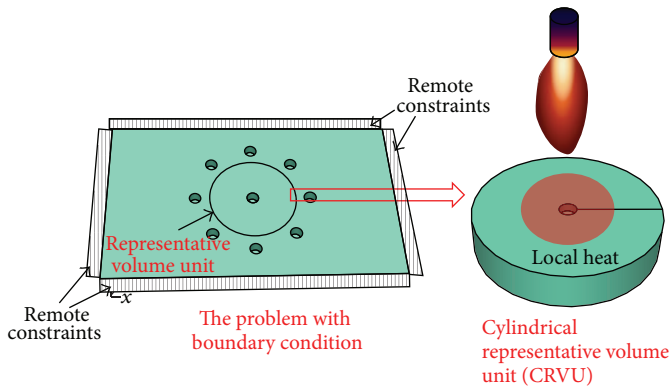

Figure 1: A schematic of a model with cylindrical representative volume unit (CRVU) subjected to local heating.

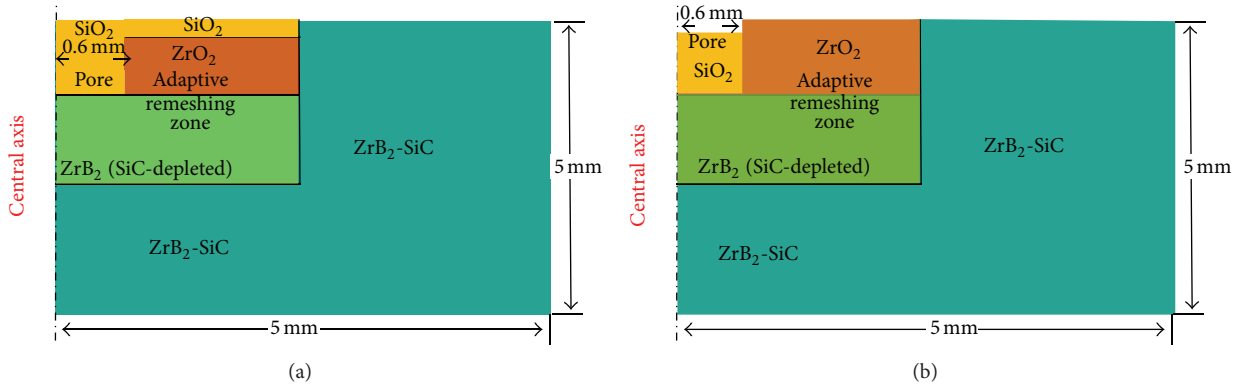

Figure 2: FEA models for ZrB_2-SiC ceramic after oxidation. (a) Lower temperature (external layer of SiO_2), and (b) higher temperature (partial evaporation of the glassy SiO_2).

and additional stress concentrations during the cool-down process from the processing temperature, thereby leading to potential cracking. Some researchers [8–12], having performed furnace oxidation and high velocity thermal shock tests on ZrB_2-SiC, have indeed shown cracking in the ZrO_2 scale.

The purpose of this study is to develop a thermal and mechanical simulation model for ZrB_2-SiC ceramics after oxidation. A steady-state heat transfer analysis was conducted using finite element analysis (FEA) modeling. An adpative remeshing technique is employed in both heat transfer and thermal stress analysis. A "global-local modeling" technique is used to combine finite element with infinite element for the thermal stress and the stress concentration analysis near a pore. Temperature, thermal, and residual stress distributions will be presented.

2. FEA Model and Simulation Procedure for ZrB_2-SiC after Oxidation

To simplify the problem, the ZrO_2 scale was assumed to be of uniform thickness with regularly distributed pores. The pores were assumed to be straight, columnar in structure without tortuosity. A cylindrical representative volume unit (CRVU) was constructed and further treated as a two-dimensional (2D, pseudo-3D) axisymmetric problem subjected to local heating as shown in Figure 1. It is assumed that the body is stress free prior to heating.

The oxide scale that forms on ZrB_2-SiC consists of an outer layer of SiO_2, a middle layer of porous ZrO_2, and a layer of SiC-depleted ZrB_2 next to the unoxidized ZrB_2-SiC [3]. Based on the chemical oxidation models [7] and the experimental observation [3], the FEA models for ZrB_2-SiC ceramic after oxidation at high temperature were created as shown in Figure 2. An adaptive remeshing zone was created to cover the SiO_2, ZrO_2, ZrB_2 (SiC-depleted) and part of the ZrB_2-SiC base near the pore. The temperature dependent dimensions of the ZrO_2 scale (crystalline oxide), glassy SiO_2, and SiC-depleted ZrB_2 layer in ZrB_2-20 vol% SiC were obtained from the chemical oxidation model [7]. The unoxidized ZrB_2-SiC ceramic is treated as a macroscale continuous solid with properties of a predetermined ratio of 4 : 1 of ZrB_2 to SiC (ZrB_2-20 vol% SiC).

The heat conduction equation for an axisymmetric problem can be expressed as

$$\rho c \frac{\partial T}{\partial t} = \frac{k}{r}\frac{\partial}{\partial r}\left(r\frac{\partial T}{\partial r}\right) + k\frac{\partial^2 T}{\partial z^2}, \quad (1)$$

where t is the time, T is the temperature, r and z are polar axis and longitudinal axis, ρ is the mass density, c is the specific

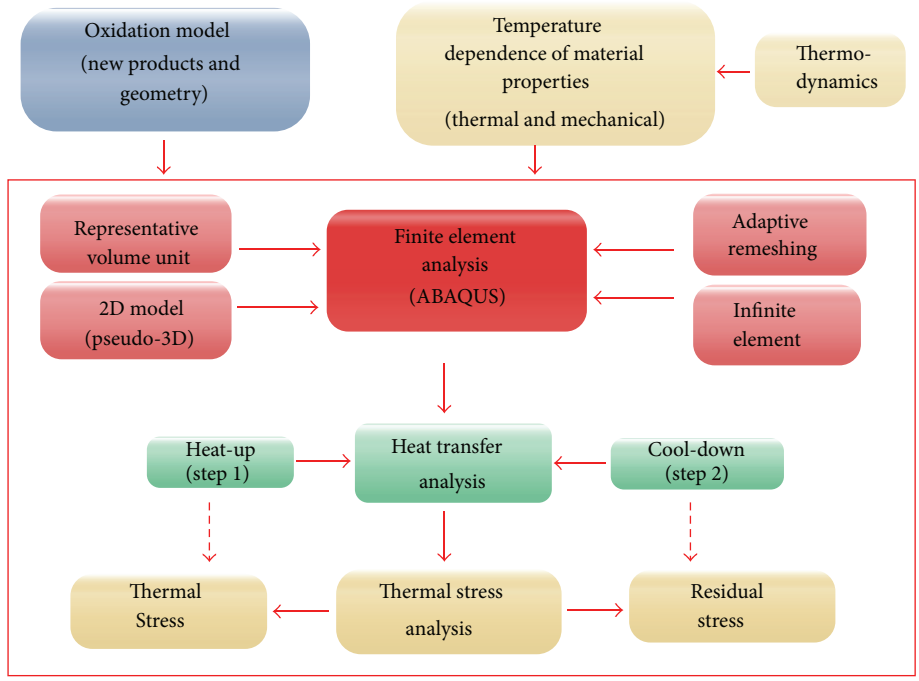

Figure 3: Flow diagram showing the procedure and steps for thermal and mechanical analyses.

heat, and k is the thermal conductivity. The thermoelastic model is given by

$$\{\sigma\} = [D]\left(\{\varepsilon\} - \{\alpha\}\,\Delta T\right), \tag{2}$$

where $[D]$ is the elasticity matrix, α the coefficient of thermal expansion, ΔT the temperature increment, σ the stress vector, and ε the strain vector.

The heat flux condition is given by

$$q = -\beta\left(T - T_0\right), \tag{3}$$

where, q is the heat flux, β is the surface film coefficient, and T_0 is the sink temperature. All simulations were conducted using ABAQUS finite element code.

The temperature dependent thermal and mechanical properties of the solid phases, needed for the heat transfer and mechanical analyses, can be found in the literature or databases [13, 14]. However, the thermal conductivity of liquid phase of SiO_2 (l) and the elastic constants cannot be found. As such, the temperature dependence of the thermal conductivity of liquid SiO_2 (l) and the elastic constants have to be predicted based on thermodynamics and some available test data. The predictive methods used for calculating the above properties are outlined in the next section. The cylindrical representative volume unit with equivalent pore diameter was treated as a 2D axisymmetric model (pseudo-3D). The modeling involves a steady-state heat transfer analysis representing local heat-up to calculate the temperature distribution and then a transient heat transfer analysis for 30 minutes representing a cool-down event to calculate the residual temperature distribution. The resulting temperature distributions were then applied to a thermomechanical finite element model to calculate the thermal stress distribution in the material. Adaptive remeshing technique was employed for the heat transfer analysis to improve accuracy. A "global-local modeling", along with the adaptive remeshing technique, is used to combine finite element with infinite element for thermal stress analysis. The procedure is summarized in Figure 3.

3. Thermal and Mechanical Properties

As mentioned earlier, the thermal conductivity and elastic constants of liquid phases of SiO_2 are not readily available. In an earlier work [15], the authors developed a method for calculating the thermal conductivity of liquid SiO_2 at a given temperature. The following thermal conductivity equation for a liquid by Hirschfelder et al. [16] is used in the method [15]:

$$k = 2.8k_B\left(\frac{A\rho\,(T)}{M}\right)^{2/3}\left(\frac{c_p}{c_V}\right)^{1/2} c_l. \tag{4}$$

In the above equation, k_B is Boltzmann's constant, n is molecules per unit volume for the liquid, A is Avogadro's number, M is molar mass, and $\rho(T)$ is the temperature dependent bulk density of the liquid, c_p and c_V are the specific heats at constant pressure and at constant volume, respectively, and c_l is speed of sound in the liquid. The temperature dependent specific heat at constant pressure, c_p, for liquid SiO_2 was reported in [14]. Then, the specific heat at constant volume, c_V, is calculated using the following relationship [17]:

$$c_V = \frac{c_p^2}{c_p + \alpha^2 T c_l^2}, \tag{5}$$

where α is the coefficient of thermal expansion. The temperature dependence of density and coefficient of thermal expansion of liquid SiO_2 were given in [18]. The speed of sound in liquids of SiO_2 was found in [19]. With all the needed parameters, the thermal conductivity of liquid SiO_2 was calculated using (4).

Using the temperature dependent values for density and speed of sound in liquid of SiO_2, the bulk and shear moduli (K, G) of liquid SiO_2 were calculated using the Newton-Laplace equation [20–24]:

$$K = \rho C_L^2; \qquad G = \rho C_T^2, \tag{6}$$

where C_L and C_T are the sound velocity of longitudinal and transverse wave, respectively. To simplify the problem, the temperature dependent elastic properties were used for the liquid phase of SiO_2 instead of the viscous properties because the stress state in liquid phase of SiO_2 was not of interest in the present study.

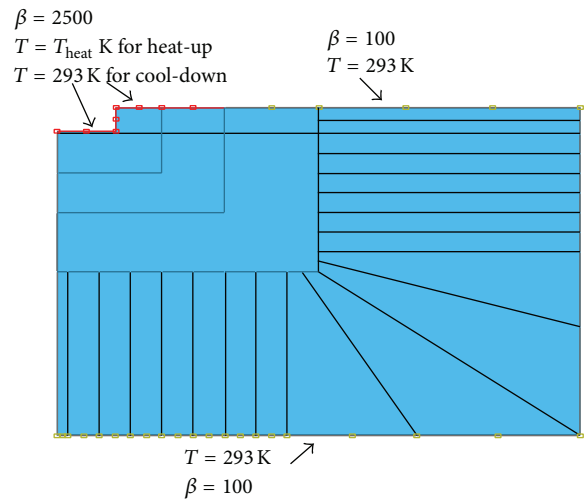

Figure 4: The heating, cooling, and sink temperature conditions used in the analysis.

4. Results and Discussions

A 2D (pseudo-3D) 4-node linear axisymmetric heat transfer quadrilateral element was used in the thermal analysis. Heat flux was used as an error indicator variable to control the adaptive remeshing rule [25]. The dimensions of the new products after oxidation were taken from the chemical oxidation model [7].

Two steps were used in the heat transfer analyses. The first step in the heat transfer analysis was a steady-state analysis representing local heating at the top surface to calculate the temperature distribution. The second step was a transient heat transfer analysis for 30 minutes representing a cooling event to room temperature to predict residual temperature distribution. The surface heating temperature was set as T_{heat} (1780 K or 2240 K) during heating and 293 K during cooling. Outside the local heating area, the sink temperature was set at 293 K. The initial temperature of the material was 293 K. The heating, cooling and sink temperature conditions are summarized in Figure 4. The surface film coefficient, β, was set as 2500 W/(m^2·K) during the heating representing a high speed fluid flow and 100 W/(m^2·K) during cooling assuming a cooler fluid flow next to a solid boundary in air. The surface film coefficient was set as 100 W/(m^2·K) at all other boundaries during both heating and cooling.

4.1. Results of Heat Transfer Analysis. The calculated temperature distributions in the body after surface heating temperatures of 1780 K and 2240 K are shown in Figures 5 and 6, respectively. In the following results, the temperatures shown in parenthesis correspond to the case of 2240 K. The maximum temperature at the top surface of the outer SiO_2 layer is 1168 K (1492 K) which is less than the applied heating temperature of 1780 K (2240 K). This is due to the effect of the surface film coefficient on heat transfer between a fluid and a solid and the thermal conduction at the boundaries. The temperatures at the interface between the outer SiO_2 layer and the ZrO_2, and at the interface between the oxide scale and ZrB_2, are 1160 K (1432 K) and 1148 K (1404 K), respectively. The temperature at the bottom surface is 1124 K (1370 K) which is much less than the heating temperature applied at the top surface. The temperatures at locations shown in Figures 5 and 6 were also calculated for different heating temperatures. The predicted temperatures in various materials and at the interfaces are linearly dependent on heating temperature, except in ZrO_2 layer. This deviation could be due to the increase in ZrO_2 layer thickness accompanied by a decrease in SiO_2 layer thickness. Figure 7 shows the predicted heat flux distribution of ZrB_2-SiC after steady-state analysis for heating to 2240 K. It is seen that a heat flux concentration occurs at the pore corner due to the geometric discontinuity and thermal conductivity mismatch.

4.2. Results of Thermal Stress Analysis. In the thermal stress analysis, the layout of infinite elements and finite elements, as well as the displacement constraints for the stress analysis shown in Figure 8, are used. The distribution of maximum principal stresses for the steady-state heating at 1780 K is shown in Figure 9(a). The maximum principal stress distribution after cooling from 1780 K is shown in Figure 9(b). The maximum value of the maximum principal stresses of 946 MPa occurs at the top surface of SiO_2 layer. The temperature at this location is about 1166 K (Figure 5), which is below the glass melting point. The brittle glassy SiO_2 is sensitive to tensile stress with an average tensile strength of 364 ± 57 MPa [26]. Therefore, a tensile stress of 946 MPa may induce cracking in the SiO_2 layer. The maximum value of the maximum principal stresses of 568 MPa occurs at the upper corner of the pore in the ZrO_2 layer and is less than the flexural strength (900 MPa) of ZrO_2 [27]. The maximum stress in the ZrB_2 is 451 MPa and occurs near the lower corner of the pore. This is higher than the measured bend strength of ZrB_2 [28]. The largest principal stress in the ZrB_2-SiC is 191 MPa, located near the lower corner of the pore. The flexural strength of ZrB_2-SiC is 1000 MPa [29–31]. For

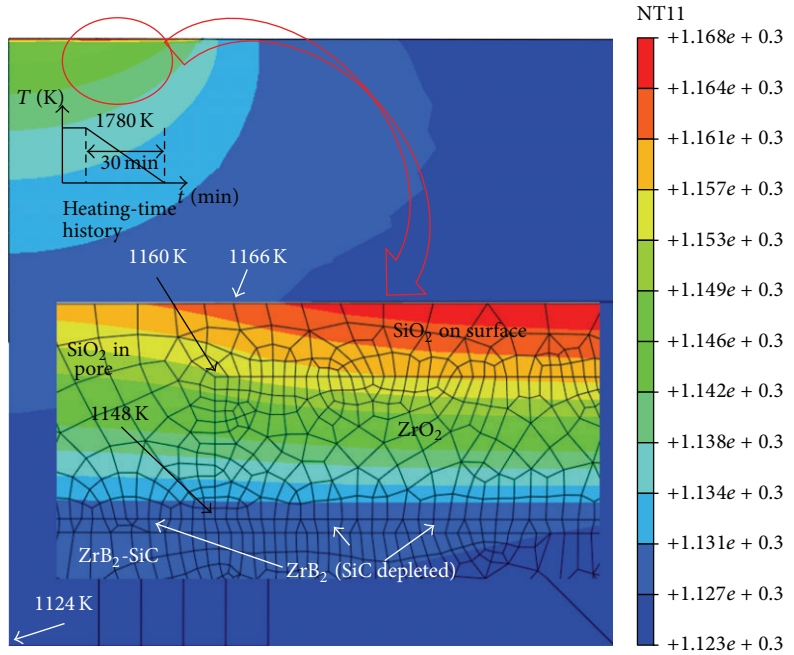

FIGURE 5: Predicted temperature distribution of ZrB_2-SiC after steady-state analysis at heating to 1780 K.

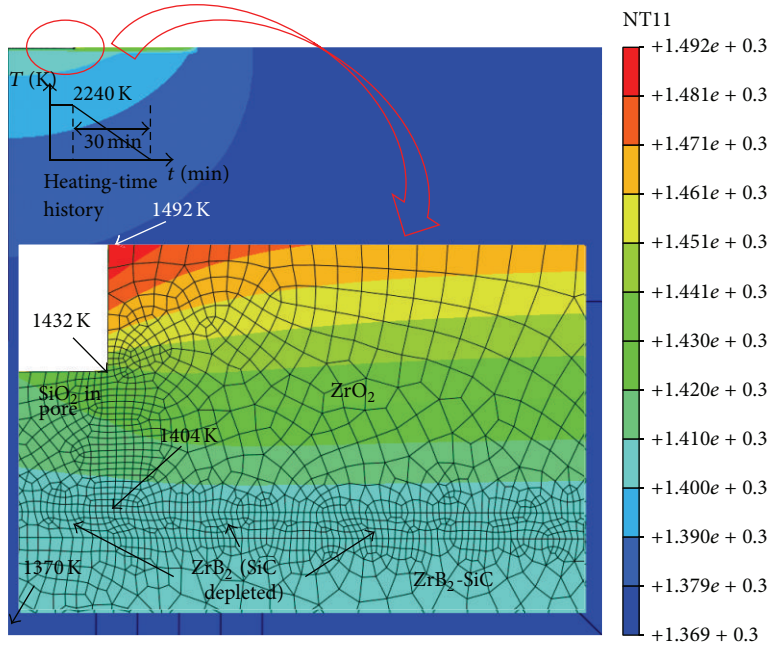

FIGURE 6: Predicted temperature distribution of ZrB_2-SiC after steady-state analysis for heating to 2240 K.

the cool-down case, the residual stresses in Figure 9(b) vary between 153 and 360 MPa.

The distribution in the maximum principal stresses near the pore for steady-state heating to 2240 K and cool-down from 2240 K to 293 K are shown in Figures 10(a) and 10(b), respectively. The stresses for heating vary between 182 and 2702 MPa while the corresponding stresses for cool-down vary between 281 and 529 MPa. Once again, the maximum values occur in the SiO_2 (2702 MPa) and ZrO_2 (2224 MPa) near the pore. This may initiate tensile cracking. These results are consistent with the experimental observations by Levine et al. [8] who performed furnace oxidation and high velocity thermal shock of ZrB_2 + 20 vol.% SiC ceramic tests. Their results show that both pores and cracks appeared in the ZrO_2 when oxidized in air at 1927°C for ten 10-min cycles. The highest maximum principal stress near the lower

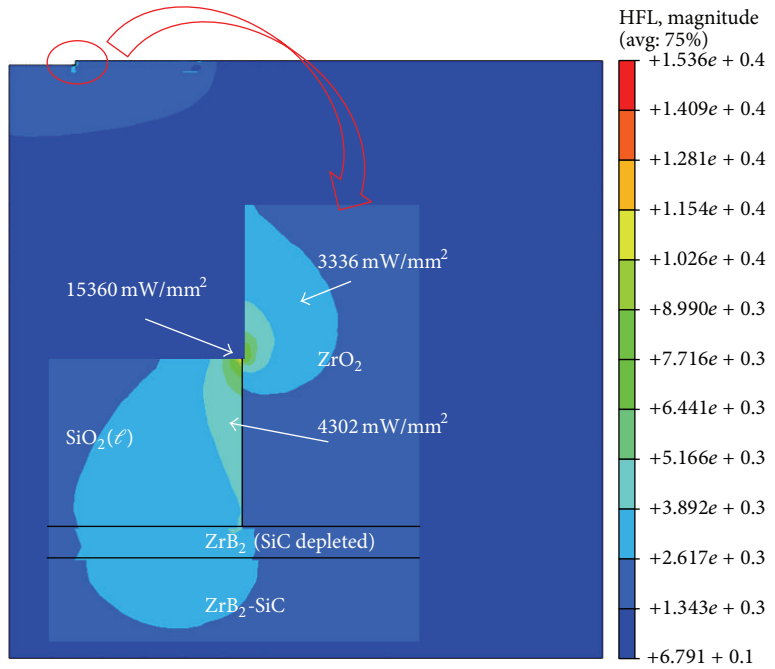

Figure 7: Predicted heat flux distribution of ZrB_2-SiC after steady-state analysis for heating to 2240 K.

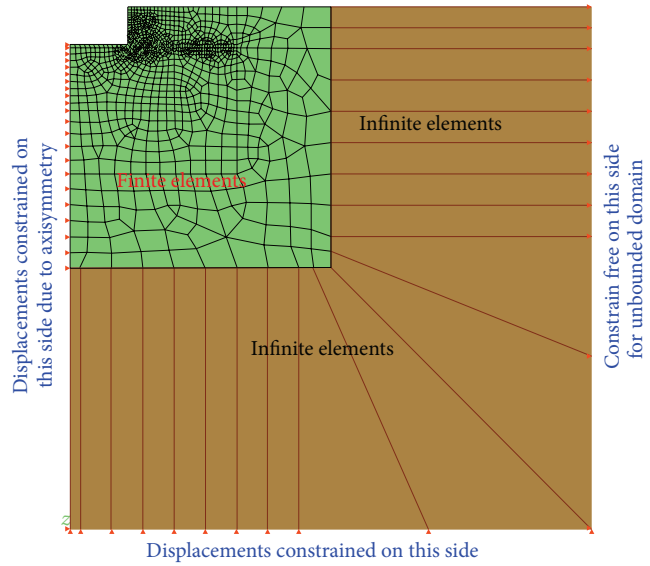

Figure 8: The infinite element, the finite element, and the boundary conditions for the thermal stress analysis.

corner of the pore in the ZrB_2 layer is 657 MPa shown in Figure 10(a) which is higher than the bending strength of the ZrB_2 as indicated above. For the cool-down case, the maximum principal stresses shown in Figure 10(b) are less than the respective material strengths except in the ZrB_2 layer.

The results were also obtained for additional temperatures. The variation of the maximum principal stress at indicated locations in Figures 9 and 10 with temperature T is shown in Figure 11(a) for heating up to T and in Figure 11(b) for cool-down from T to 293 K. The thermal stress at heating temperature T in the ZrB_2-SiC matrix is relatively small and does not vary much with heating temperature T (Figure 11(a)). The residual stress at 293 K (Figure 11(b)) in the ZrB_2-SiC decreases with the increasing heating temperature T. Watts et al. [32] measured thermal residual stresses in ZrB_2 -30 vol% SiC composites using neutron diffraction. Their results indicated that stresses begin to accumulate at about 1673 K during cool-down from the processing temperature of 2172 K. The stress increased to an

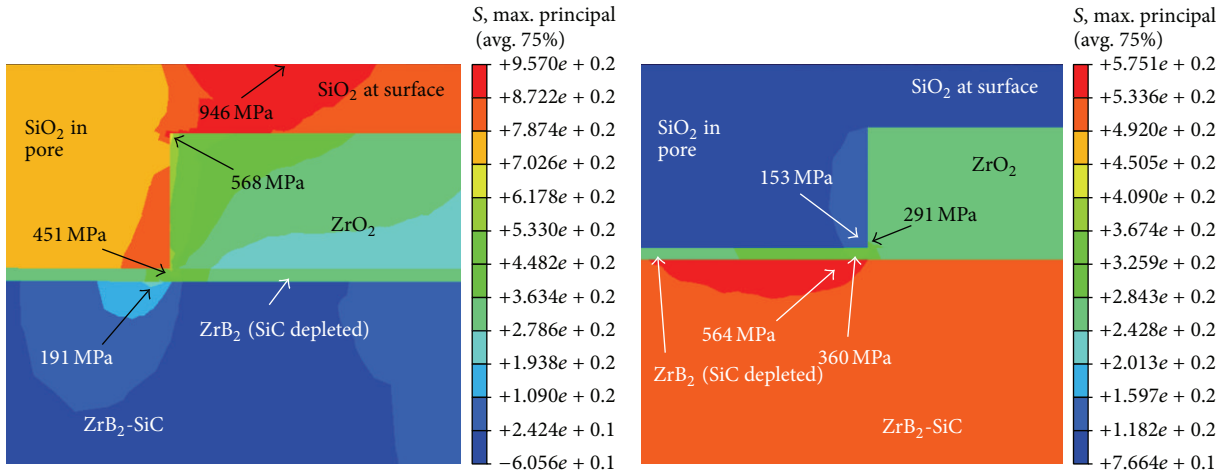

(a) Heating-up (b) Cool-down

Figure 9: Maximum principal stresses distribution in the enlarged area near pore after steady-state thermal analysis at 1780 K.

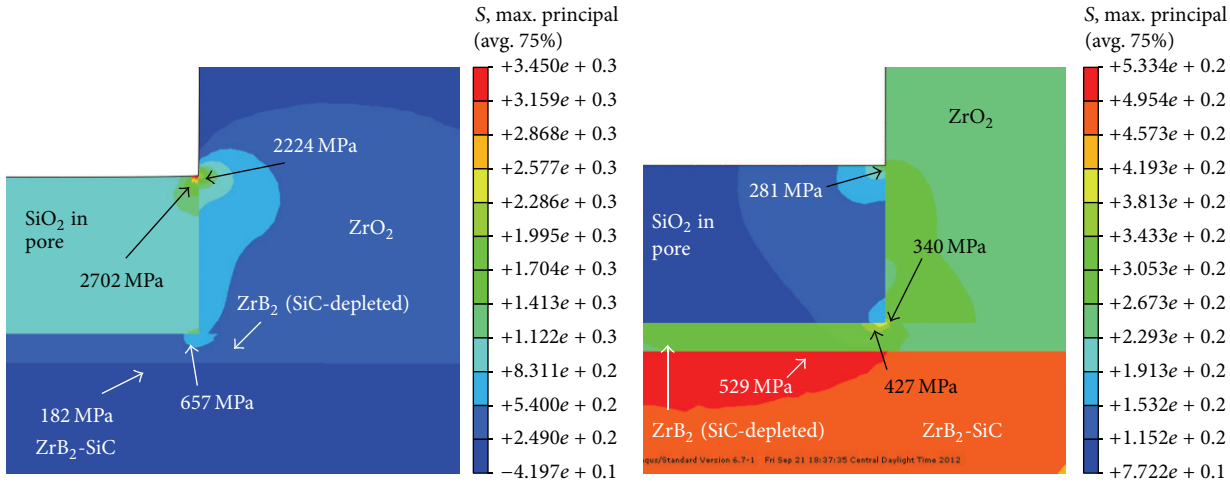

(a) Heating-up (b) Cool-down

Figure 10: Maximum principal stresses distribution in the enlarged area near pore after steady-state thermal analysis at 2240 K.

average compressive stress of 880 MPa in the SiC phase and to an average tensile stress of 450 MPa in the ZrB_2 phase. By using the rule of mixtures for 34 vol% SiC, the stress in the SiC (880 MPa) converts to an equivalent stress of 453 MPa which is very close to the measured stress of 450 MPa [32].

5. Conclusion

A "global-local modeling" technique is used combining finite element with infinite element for thermal stress analysis for the oxidation effects on heat transfer and mechanical behavior of ZrB_2-SiC ceramics at high temperature. Thermal conductivity was calculated for the liquid phase of SiO_2 based on a theoretical formulation. The predicted temperature at the top surface of the outer SiO_2 layer is less than the applied heating temperature due to the surface film coefficient effect on the heat transfer between a fluid and a solid and the thermal conduction at the boundaries. An increase in ZrO_2 layer thickness, accompanied by a decrease in SiO_2 layer thickness, during oxidation will affect heat transfer in the body. Heat flux concentration occurs at the pore corner due to the geometric discontinuity and the material property mismatch. Thermal and residual stress concentrations occur near the pore due to geometric discontinuity and the material properties mismatch between the ceramic matrix and the new products. Thermal stresses in the surface oxide layers consisting of SiO_2 and ZrO_2, are higher than their respective materials strengths. Thermal and residual stresses in the layer

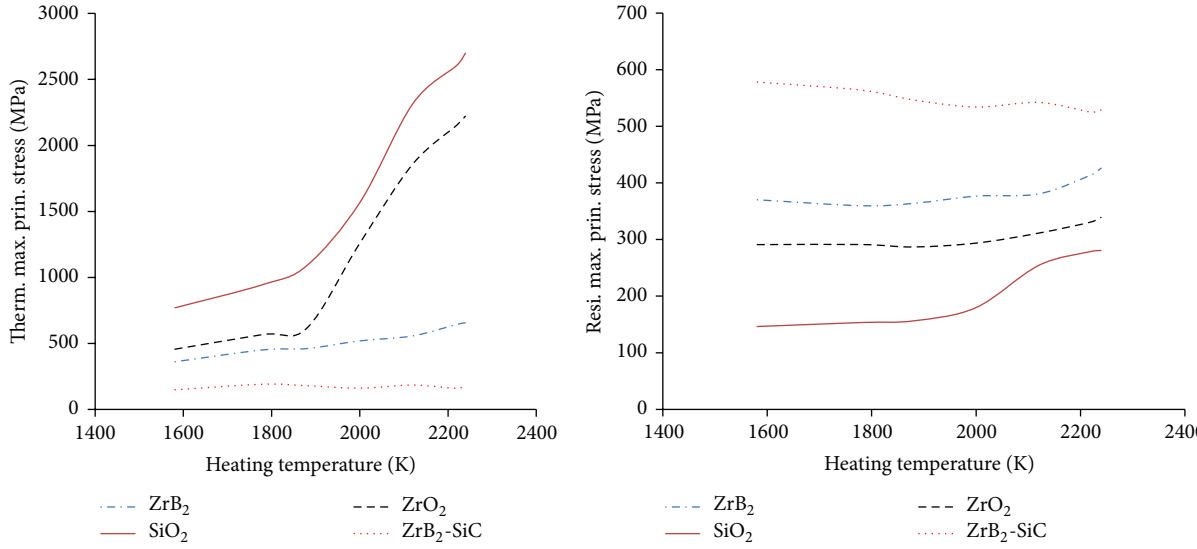

(a) Thermal stress

(b) Residual stress

Figure 11: Thermal and residual maximum principal stress at indicated locations for different heating temperatures.

of a new oxidation product of SiC-depleted ZrB_2 layer for both heating and cooling cases are higher than the material strength. Therefore, it is expected that damage may initiate in the layers of new oxidation products.

Conflict of Interests

The authors declare that there is no conflict of interests regarding the publication of this paper.

Acknowledgments

This project was funded under subcontract 10-S568-0094-01-C1 through the Universal Technology Corporation under prime contract number FA8650-05-D-5807. The authors are grateful to the technical support on the program by the Air Force Research Laboratory and specifically to Dr. Mike Cinibulk at AFRL for both his collaboration and guidance.

References

[1] M. M. Opeka, I. G. Talmy, and J. A. Zaykoski, "Oxidation-based materials selection for 2000°C + hypersonic aerosurfaces: theoretical considerations and historical experience," *Journal of Materials Science*, vol. 39, no. 19, pp. 5887–5904, 2004.

[2] W. G. Fahrenholtz, G. E. Hilmas, A. L. Chamberlain, and J. W. Zimmermann, "Processing and characterization of ZrB_2-based ultra-high temperature monolithic and fibrous monolithic ceramics," *Journal of Materials Science*, vol. 39, no. 19, pp. 5951–5957, 2004.

[3] W. G. Fahrenholtz, "Thermodynamic analysis of ZrB_2-SiC oxidation: formation of a SiC-depleted region," *Journal of the American Ceramic Society*, vol. 90, no. 1, pp. 143–148, 2007.

[4] C. M. Carney, P. Mogilvesky, and T. A. Parthasarathy, "Oxidation behavior of zirconium diboride silicon carbide produced by the spark plasma sintering method," *Journal of the American Ceramic Society*, vol. 92, no. 9, pp. 2046–2052, 2009.

[5] W. G. Fahrenholtz, "The ZrB_2 volatility diagram," *Journal of the American Ceramic Society*, vol. 88, no. 12, pp. 3509–3512, 2005.

[6] A. Rezaie, W. G. Fahrenholtz, and G. E. Hilmas, "Evolution of structure during the oxidation of zirconium diboride-silicon carbide in air up to 1500∘C," *Journal of the European Ceramic Society*, vol. 27, no. 6, pp. 2495–2501, 2007.

[7] T. A. Parthasarathy, R. A. Rapp, M. Opeka, and M. K. Cinibulk, "Modeling oxidation kinetics of SiC-containing refractory diborides," *Journal of the American Ceramic Society*, vol. 95, no. 1, pp. 338–349, 2012.

[8] S. R. Levine, E. J. Opila, M. C. Halbig, J. D. Kiser, M. Singh, and J. A. Salem, "Evaluation of ultra-high temperature ceramics for aeropropulsion use," *Journal of the European Ceramic Society*, vol. 22, no. 14-15, pp. 2757–2767, 2002.

[9] J. C. Han, P. Hu, X. Zhang, S. Meng, and W. Han, "Oxidation-resistant ZrB2-SiC composites at 2200°C," *Composites Science and Technology*, vol. 68, no. 3-4, pp. 799–806, 2008.

[10] X.-H. Zhang, P. Hu, and J.-C. Han, "Structure evolution of ZrB_2-SiC during the oxidation in air," *Journal of Materials Research*, vol. 23, no. 7, pp. 1961–1972, 2008.

[11] P. Hu, W. Guolin, and Z. Wang, "Oxidation mechanism and resistance of ZrB_2-SiC composites," *Corrosion Science*, vol. 51, no. 11, pp. 2724–2732, 2009.

[12] P. Sarin, P. E. Driemeyer, R. P. Haggerty et al., "In situ studies of oxidation of ZrB2 and ZrB2–SiC composites at high temperatures," *Journal of the European Ceramic Society*, vol. 30, no. 11, pp. 2375–2386, 2010.

[13] "Material Property Database (MPDB)," JAHM Software, Inc., http://www.jahm.com.

[14] I. Barin, *Thermochemical Data of Pure Substances*, Wiley-VCH, New York, NY, USA, 3rd edition, 1995.

[15] J. Wei, L. R. Dharani, K. Chandrashekhara, G. E. Hilmas, and W. G. Fahrenholtz, "Modeling of oxidation effects on heat transfer behavior of ZrB_2 and ZrB_2-SiC Ceramics at high temperature,"

in *Proceedings of the 53rd AIAA/ASME/ASCE/AHS/ASC Structures, Structural Dynamics and Materials Conference*, AIAA, Honolulu, Hawaii, USA, April 2012.

[16] J. O. Hirschfelder, C. F. Curtiss, and R. B. Bird, *Molecular Theory of Gases and Liquid*, John Wiley & Sons, New York, NY, USA, 1954.

[17] R. S. Hixson, M. A. Winkler, and J. W. Shaner, "Sound speed measurements in liquid lead at high temperature and pressure," in *Conference: 10. High Pressure Conference on Research in High Pressure Science and Technology*, Amsterdam, The Netherlands, 1985, LA-UR-85-2363.

[18] M. S. Ghiorso, "An equation of state for silicate melts. I. Formulation of a general model," *American Journal of Science*, vol. 304, no. 8-9, pp. 637–678, 2004.

[19] A. Polian, V.-T. Dung, and P. Richet, "Elastic properties of a-SiO_2 up to 2300 K from Brillouin scattering measurements," *Europhysics Letters*, vol. 57, no. 3, pp. 375–381, 2002.

[20] 2013, https://en.wikipedia.org/wiki/Speed_of_sound.

[21] D. D. Joseph, A. Narain, and O. Riccius, "Shear-wave speeds and elastic moduli for different liquids. Part 1. Theory," *Journal of Fluid Mechanics*, vol. 171, pp. 289–308, 1986.

[22] D. D. Joseph, O. Riccius, and M. Arney, "Shear-wave speeds and elastic moduli for different liquids. Part 2: experiments," *Journal of Fluid Mechanics*, vol. 171, pp. 309–338, 1986.

[23] O. Riccius, D. D. Joseph, and M. Arney, "Shear-wave speeds and elastic moduli for different liquids Part 3. Experiments-update," *Rheologica Acta*, vol. 26, no. 1, pp. 96–99, 1987.

[24] M. S. Greenwood and J. A. Bamberger, "Measurement of viscosity and shear wave velocity of a liquid or slurry for on-line process control," *Ultrasonics*, vol. 39, no. 9, pp. 623–630, 2002.

[25] "ABAQUS 6.9 documentation," http://www.simulia.com/support/documentation.html.

[26] W. N. Sharpe Jr., J. Pulskamp, D. S. Gianola, C. Eberl, R. G. Polcawich, and R. J. Thompson, "Strain measurements of silicon dioxide microspecimens by digital imaging processing," *Experimental Mechanics*, vol. 47, no. 5, pp. 649–658, 2007.

[27] http://www.ferroceramic.com/zirconia.htm.

[28] D. Kalish, E. V. Clougherty, and K. Kreder, "Strength, fracture mode, and thermal stress resistance of HfB_2 and ZrB_2," *Journal of the American Ceramic Society*, vol. 52, no. 1, pp. 30–36, 1969.

[29] A. L. Chamberlain, W. G. Fahrenholtz, G. E. Hilmas, and D. T. Ellerby, "High-strength zirconium diboride-based ceramics," *Journal of the American Ceramic Society*, vol. 87, no. 6, pp. 1170–1172, 2004.

[30] A. Rezaie, W. G. Fahrenholtz, and G. E. Hilmas, "Effect of hot pressing time and temperature on the microstructure and mechanical properties of ZrB_2-SiC," *Journal of Materials Science*, vol. 42, no. 8, pp. 2735–2744, 2007.

[31] S. Zhu, W. G. Fahrenholtz, and G. E. Hilmas, "Influence of silicon carbide particle size on the microstructure and mechanical properties of zirconium diboride-silicon carbide ceramics," *Journal of the European Ceramic Society*, vol. 27, no. 4, pp. 2077–2083, 2007.

[32] J. Watts, G. Hilmas, W. G. Fahrenholtz, D. Brown, and B. Clausen, "Measurement of thermal residual stresses in ZrB_2-SiC composites," *Journal of the European Ceramic Society*, vol. 31, no. 9, pp. 1811–1820, 2011.